Jacobian-determinant method of identifying phase singularity during reentry

Teng-Chao Li,[1] De-Bei Pan,[1] Kuangshi Zhou,[2] Ruhong Jiang,[2] Chenyang Jiang,[2] Bo Zheng,[1,3,*] and Hong Zhang[1,†]
[1]*Zhejiang Institute of Modern Physics and Department of Physics, Zhejiang University, Hangzhou 310027, China*
[2]*Department of Cardiology, Sir Run Run Shaw Hospital, School of Medicine, Zhejiang University, Hangzhou 310016, China*
[3]*Collaborative Innovation Center of Advanced Microstructures, Nanjing 210093, China*

(Received 8 April 2018; revised manuscript received 13 October 2018; published 11 December 2018)

Reentrant spiral waves (also called rotors) have been observed in the heart muscle during cardiac arrhythmias and are nowadays targeted by ablation therapy in order to cure certain heart rhythm disorders. Phase singularity (PS) is considered to represent the organizing center of the spiral wave and the spatiotemporal behavior of the spiral wave can be extensively quantified by tracking PS. Recent clinical studies suggested that ablating the tissue at PS locations may cure atrial fibrillation. However, for experimental data, typically only one state variable, i.e., the voltage, is recorded. Accordingly, the calculation of phase and the identification of PSs must be carried out by using one variable. Here, a Jacobian-determinant method using one variable in reconstructed state space is proposed and the advantages of the method are demonstrated.

DOI: 10.1103/PhysRevE.98.062405

I. INTRODUCTION

Spiral waves are one of the most striking spatiotemporal patterns existing in diverse physical, chemical, and biological systems. They have been observed in the Belousov-Zhabotinsky (BZ) reaction [1,2], in the catalytic oxidation of CO on platinum [3], during the aggregations of *Dictyostelium discoideum* amoebae [4], and in the cardiac tissue [5–7]. Due to the close relevance to cardiac diseases such as tachycardia and fibrillation, such kinds of patterns have raised broad interest [8–10]. The global behavior of a spiral is quite complex, but some features can be well described by the motion of its rotation center and the center is usually defined by a phase singularity (PS). A PS is a site at which the phase of the site is arbitrary; the neighboring elements exhibit a continuous progression of phase that is equal to $\pm 2\pi$ around this site [11].

The transition from a stable to a drifting or meandering PS trajectory and then to spiral wave breakup may correspond to the transition from stable to polymorphic electrical arrhythmias and then to fibrillation which leads to sudden cardiac death [12,13], such that the accurate identification of the PS is particularly important in the heart. Recently, Narayan and colleagues have suggested that ablating the tissue at PS locations may cure fibrillation of the cardiac atria [14].

A classic method to determine the PS location is to compute where the isocontours of two-state variables intersect [15–18]. This method allows for the identification of PS at each instant of time but suffers from the lack of clear criteria for selecting the particular isocontour and the necessity to know the spatiotemporal behavior of two-state variables. Though robust and suitable for numerical simulations, this method is not applicable to experimental data, for which typically only one dependent variable (generally voltage V) is recorded.

A similar method involves choosing a particular choice of isocontour value or an origin V^* in state space, and the site of maximal wave-front curvature can be used to track PS movement [19]. This approach alleviates the need for two-state variables, since only the transmembrane potential isocontour is used but again requires the choice of a particular isopotential. However, the particular isopotential establishment is crucial for appropriate tracking of the PS of rapidly rotating waves [20]. Moreover, by using this method, the sites of maximal curvature on concave wave fronts, i.e., "inner points" that cannot be PSs, are also identified as PSs. Alternatively, the so-called zero-normal-velocity method [21] consists of finding the point on a chosen isopotential line which exhibits a zero time derivative. This method has been used in many settings including experiments [22–25].

The subsequent methods use a time delay–embedding technique to calculate phase ϕ from a two-dimensional reconstructed state space, which is topologically equivalent to the true state space [26], and the identification of PS has been carried out manually using one variable [11]. In Ref. [27], the authors demonstrated that the phase can be calculated by using the Hilbert transform–based approach, which also alleviates the need for two-state variables.

Phase maps $\phi(x, y, t)$ can be obtained by using the above methods to calculate phase at every site (x, y) of the spiral wave for each instant of time t. A spatial PS occurs at a site where all phase values converge. Iyer and Gray developed an algorithm to locate PS during reentry by computing the line integral of the change of the phase around each pixel [28]. Bray *et al.* [29] used a convolution method to locate PS: The concept of topological charge is implemented as a series of convolution operations to detect a spatial phase distribution of 2π around a pixel, the distinguishing characteristic of a PS. Recently, a location-centric method that looks for the phase discontinuity point at which PS occurs was proposed

*zhengbo@zju.edu.cn
†hongzhang@zju.edu.cn

by Lee *et al.* [30]. The authors emphasized that their method is limited on the condition that voltage changes continuously over time. Note that the above methods require calculating the local phase $\phi(x, y, t)$, while the definition of the phase can vary from study to study.

In this paper, we propose an alternative method of PS identification, i.e., the Jacobian-determinant method. The method is performed in a reconstructed state space, such that only one variable is needed. Furthermore, the phase does not need to be calculated in this method. We illustrate the principle of this method and a comparison with other methods is given.

II. METHODS

A. Two-state variable model

We now consider a classic two-variable FitzHugh-Nagumo (FHN) model [31,32],

$$\frac{\partial V}{\partial t} = \frac{1}{\varepsilon}\left(V - \frac{V^3}{3} - W\right) + D\nabla^2 V, \tag{1a}$$

$$\frac{\partial W}{\partial t} = \varepsilon(V + \beta - \gamma W), \tag{1b}$$

where V and W are fast and slow variables, respectively; D is the diffusion coefficient; and ε, β, and γ are model parameters. In this paper, Eq. (1) is integrated on a uniform $x-y$ grid with no-flux boundary conditions via the Euler algorithm. Numerical simulations are conducted by using fixed steps $\Delta x = \Delta y = 0.05$ and $\Delta t = 0.0005$. The size of the system is $Lx = Ly = 25$, consisting of 500×500 grid points.

B. Jacobian-determinant method

For numerical simulations, phase can be directly achieved from the two-state variables. Due to normally only one variable, i.e., voltage V, being recorded in experiments, the calculation of phase using one variable has already been accomplished by using a reconstructed state space [11,26]. The phase can be calculated by using the time delay–embedding technique from a two-dimensional reconstructed state space as follows:

$$\phi(x, y, t) = \arctan 2[V(t+\tau) - V^*, V(t) - V^*]. \tag{2}$$

The arctan 2 function returns a value of phase between $-\pi$ and π depending upon the value and signs $(+/-)$ of the two input variables. The constant V^* is the origin of the phase space and the best choice of V^* can be computed numerically whether the spiral wave is stationary or not [33].

The phase can also be calculated by using the Hilbert transform–based approach [27]:

$$\phi(x, y, t) = \arctan 2(V'(t), H[V'(t)]),$$

where $V'(t) = V(t) - V_{\text{mean}}(t)$ and H is the Hilbert transform. One advantage of this approach is that it does not require a judicial choice of τ in Eq. (2). However, the signal must meet some conditions for reliable phase computation: Techniques that use the Hilbert transform approach must ensure that the mean potential over each activation cycle is subtracted from the original electrogram for reliable phase computations [34].

Phase analysis of cardiac arrhythmias, particularly atrial fibrillation, has gained interest because of the ability to detect organized stable spirals and target them for therapy. However, the lack of methodology details in publications on the topic has resulted in ongoing debate over the phase mapping technique [35,36]. Bray and Wikswo [27] also pointed out that globally choosing a short τ for the time delay–embedding method (2) achieves the same desired effect in the phase plane as the orthogonality of the Hilbert-transformed signal. Thus, for simplicity, we will discuss the PS by using Eq. (2) in the following, where the phase is calculated by using the time delay–embedding technique.

PS can then be described in terms of topological charge [37–39], which is defined as

$$n_t = \frac{1}{2\pi}\oint_\Gamma \nabla\phi \cdot d\vec{l}, \tag{3}$$

where Γ is a closed curve surrounding the PS. A PS occurs when the line integral of the change of phase around a point is 2π or -2π, i.e., $n_t = 1$ or -1, which depends on the chirality of a spiral [40,41].

Following the topological current theory [40–43], it can be proven that

$$n_t = \text{sgn}[D(V/x)_{\text{PS}}], \tag{4}$$

where $D(V/x)$ is the Jacobian determinant,

$$D(V/x) = \left[\frac{\partial V(t)}{\partial x}\frac{\partial V(t+\tau)}{\partial y} - \frac{\partial V(t)}{\partial y}\frac{\partial V(t+\tau)}{\partial x}\right]. \tag{5}$$

$D(V/x)_{\text{PS}}$ is the value of $D(V/x)$ at the PS.

First, we consider meandering (nonstationary) spiral waves. Spatial distributions of the fast variable V at an instant time $t = 90$ are shown in Fig. 1(a). According to Eq. (5), we numerically calculated the values of the Jacobian determinant $D(V/x)$, as shown in Fig. 1(b). For a counterclockwise spiral, one can see that $D(V/x)$ is localized at the PS: $D(V/x)$ takes its maximum value approximately at the PS ($n_t = \text{sgn}[D(V/x)_{\text{PS}}] = +1$), while it is almost zero in other regions. Note that for a clockwise spiral, the PS is distinguished by its sharp local minimum of $D(V/x)$: $D(V/x)$ takes its minimum value approximately at the PS ($n_t = \text{sgn}[D(V/x)_{\text{PS}}] = -1$). The property that the Jacobian determinant $D(V/x)$ is localized at the PS provides an identification of the PS position for a counterclockwise (or clockwise) spiral by maximizing (or minimizing) $D(V/x)$.

In Fig. 1(c), the middle red and blue isolines are the values of $V(t)$ and $V(t+\tau)$ of the grid that reaches the maximum of $D(V/x)$, respectively. Hence, the intersection of these two middle lines is identified as the PS, which is denoted by a green circle in a zoomed-in image in Fig. 1(d). $\nabla V(t)$ and $\nabla V(t+\tau)$ are vectors denoted by the red and the blue arrows in Fig. 1(d). Specifically, $D(V/x) = |\nabla V(t)| \cdot |\nabla V(t+\tau)| \cdot \sin\theta$ $(-\pi < \theta \leqslant \pi)$, where θ is the angle between the vectors $\nabla V(t)$ and $\nabla V(t+\tau)$ and is measured in the counterclockwise direction from the vector $\nabla V(t)$. One can see the values of $D(u/x)$ depend on three variables, i.e., $|\nabla V(t)|$, $|\nabla V(t+\tau)|$, and θ. Far away from the PS, the two vectors $\nabla V(t)$ and $\nabla V(t+\tau)$ are almost parallel to each other and thus $D(V/x)$ is nearly zero, while near the PS,

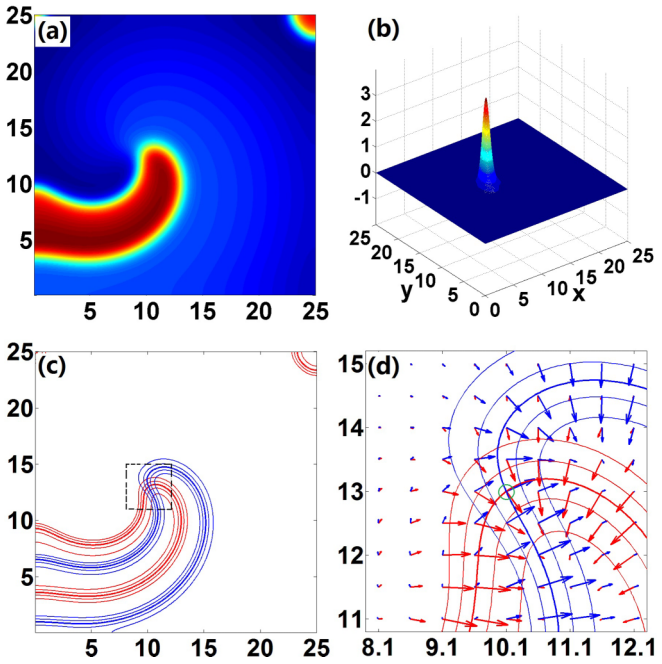

FIG. 1. FHN model with $\varepsilon = 0.22$, $\beta = 0.70$, and $\gamma = 0.80$ is used; a time delay $\tau = 0.1T$ and an instant time $t = 90$ are chosen, where $T = 13.114$ is the rotation period of the spiral. (a) A snapshot of the spatial distribution of the fast variable V. (b) Numerical values of the Jacobian determinant $D(V/x)$. (c) The middle red isoline $V(t) = 0.377$ is the value of V of the grid that reaches the maximum of $D(V/x)$ in (b), and the other four red isolines are $V(t) \pm \Delta V$ and $V(t) \pm 2\Delta V$. Similarly, the middle blue isoline and the other four blue isolines correspond to $V(t+\tau) = 0.09$, $V(t+\tau) \pm \Delta V$, and $V(t+\tau) \pm 2\Delta V$, respectively. $\Delta V = 0.5$ is chosen in both the red and blue cases. (d) The region enclosed by black dashed lines in (c) is zoomed in. The red and blue arrows are vectors that denote $\nabla V(t)$ and $\nabla V(t+\tau)$, respectively, and the arrows point to the directions where V increase. The green circle is the center of the image, which also corresponds to the grid that reaches the maximum of $D(V/x)$.

$\nabla V(t)$ and $\nabla V(t+\tau)$ cross each other and $D(V/x)$ takes its maximum value at the PS.

C. Other methods

Gray *et al.* [33] showed that inappropriate origin choice can lead to an error in the identification of the number and lifetime of spiral waves, and the best choice of the state space origin was discussed. They first considered a stable, i.e., rigidly rotating (stationary), spiral wave since such a spiral wave exhibits rotational symmetry around the center of rotation, which can be denoted as (x^*, y^*) in Cartesian coordinates. At each site (x, y) the state variables will be periodic in time except at the site (x^*, y^*) where no oscillations occur because of the rotational symmetry. They suggested that the best choice of the state space origin for the definition of ϕ [see Eq. (2)] is the value of the state variable at (x^*, y^*) defined as V^*. If the site (x^*, y^*) is chosen for the definition of PS identification, then the PS trajectory during one rotation will be a point. Gray *et al.* further showed that one can seek a rotationally symmetric spiral wave solution in a polar coordinate system [44], under such circumstance the state at the center of this spiral wave

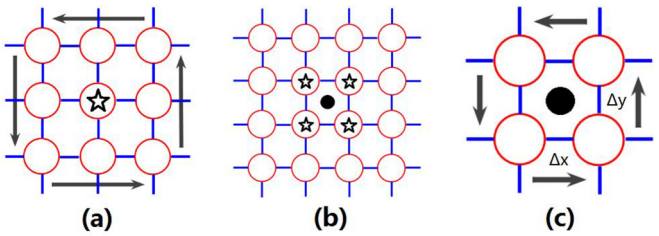

FIG. 2. Schematic representation of the simplified phase-integral method [47]. The change in phase between two adjacent points ranges from $-\pi$ to π. (a) The phase-integral method calculates the line integral of the change in phases at a candidate point with its eight neighbor points. (b) Four points indicated by the stars are identified as PSs by the phase-integral method and the real PS exists at the intersection of these four points. (c) The simplified phase-integral method. Only four points are required to calculate the line integral and the center of the four points is considered as a PS candidate.

solution V^* can be computed numerically whether the spiral wave is stationary or not, and the center of rotation (x^*, y^*) in Cartesian coordinates becomes $\rho = 0$ in the polar coordinate system.

In this paper, we use the open source software DXSPIRAL [45,46] since it is dealing with spiral waves on a polar grid in a disk. V^* can be obtained at $\rho = 0$ and the rotation period of the spiral T can also be given. To get a similar precision with $\Delta x = 0.05$ in direct numerical simulations, we use a disk of radius of 12.5 with 250 radial and 124 circumferential grid cells. We have obtained $V^* = -1.139$ with the chosen model parameters as described in Fig. 1, which is consistent with the result given by Gray *et al.* in Table I of Ref. [33].

With the phase-integral method [28], PS is calculated based on the line integral of the phase around a PS point equal to $\pm 2\pi$ [see Eq. (3)]. The path length of the line integral can be varied. Apparently a smaller path length is of more desirable precision. The phase-integral method [28] uses a path length of eight points as shown in Fig. 2(a), and tracks as many as four PSs at one time, which are denoted by the black star in Fig. 2(b), and the real PS lies at the common junction of these four points indicated by a black dot. In this paper, we adopted the simplified phase-integral method [47]: by using a path length of only four points and the center of the four points is considered as a PS candidate, which is denoted by a black dot as one can see in Fig. 2(c). Our numerical simulations with spiral waves in both meandering and rigidly rotating cases showed that the phase-integral method and the simplified phase-integral method are equivalent, and that the latter one is time saving.

For comparison, the third method we use for the identification of a PS is the convolution method developed by Bray *et al.* [29]. They demonstrated that the line integral of Eq. (3) at location (x, y) can be solved by making the following convolution operation:

$$\oint_\Gamma \nabla\phi \cdot d\vec{l} \propto \nabla_x \otimes k_y + \nabla_y \otimes k_x, \tag{6}$$

where $k_x = \phi(x + \Delta x, y) - \phi(x, y)$, $k_y = \phi(x, y + \Delta y) - \phi(x, y)$, $\otimes$ is the convolution operator, and ∇_x, ∇_y are the convolution kernels. In this paper, we use an updated set

of convolution kernels discussed in [20]. The line integral in Eq. (3) divided by 2π would not be exactly ± 1 due to discretization error, so we use an absolute margin of error with 0.001 [48].

The fourth method is the location-centric method which was proposed by Lee *et al.* [30]. They selected the PS only based on the phase difference $\Delta\phi = \phi(t+1) - \phi(t)$ at a local site without checking the phase changes at the site's neighbor points, where $\phi(t)$ is the phase at time t. A candidate site is considered as the PS if the phase difference satisfies the condition $\Delta\phi < M$, where M is set to $-\pi$.

The fifth method is the zero-normal-velocity method developed by Fenton and Karma [21]. In this method, the PS can be defined as the point where the excitation wave front meets the repolarization wave back of the action potential, or equivalently as the point of zero normal velocity along the boundary between depolarized and repolarized regions of the cardiac tissue. It is simple to show that this point is the intersection point of the lines,

$$V(x, y, t) = V^*, \quad \partial_t V(x, y, t) = 0. \tag{7}$$

The equivalence of the phase-integral and the zero-normal-velocity approaches has been demonstrated experimentally [22]. In this paper, we call Eq. (7) the zero-normal-velocity method I. In the Appendix, we proved that the zero-normal-velocity method I is equivalent to the phase-integral method (3) when the time delay τ is extremely small; i.e., $\tau \ll 1$.

In practice, especially in experiments, $\partial_t V(x, y, t)$ is calculated roughly from $[V(x, y, t+\tau) - V(x, y, t)]/\tau$. In this case, the method (7) changes to

$$V(x, y, t) = V^*, \quad V(x, y, t+\tau) - V(x, y, t) = 0, \tag{8}$$

which we call the zero-normal-velocity method II and is equivalent to the phase-integral method (3) (more details can be found in the Appendix).

III. RESULTS

A. Comparison with other methods

Now we compare the PS locations determined by the Jacobian-determinant method with other five methods. To produce the PS trajectory by each method, we calculate PS points in a time duration 100 and the time interval of the PS detection is 1; we define the PS-detecting error rate as the number of false results (false-positive plus false-negative PSs) divided by the total number of true PSs [20]. The simplified phase-integral method, the convolution method, the Jacobian-determinant method, the zero-normal-velocity method II, and the zero-normal-velocity method I, whose PS trajectories are shown in Figs. 3(a), 3(b), and 3(d)–3(f), respectively, have a 0 error rate of the PS detection. Nevertheless in Fig. 3(c), the location-centric method is of 67% error rate.

We also explored the effects of different choices of time delay τ in the PS identification. In the meandering (nonstationary) case, the PS-detecting error rates of different methods are shown in Table I. One can see that the simplified phase-integral method, the convolution method, the Jacobian-determinant method, and the zero-normal-velocity method II have a 0 error rate of the PS detection with different time delays while the location-centric method is of high error rate.

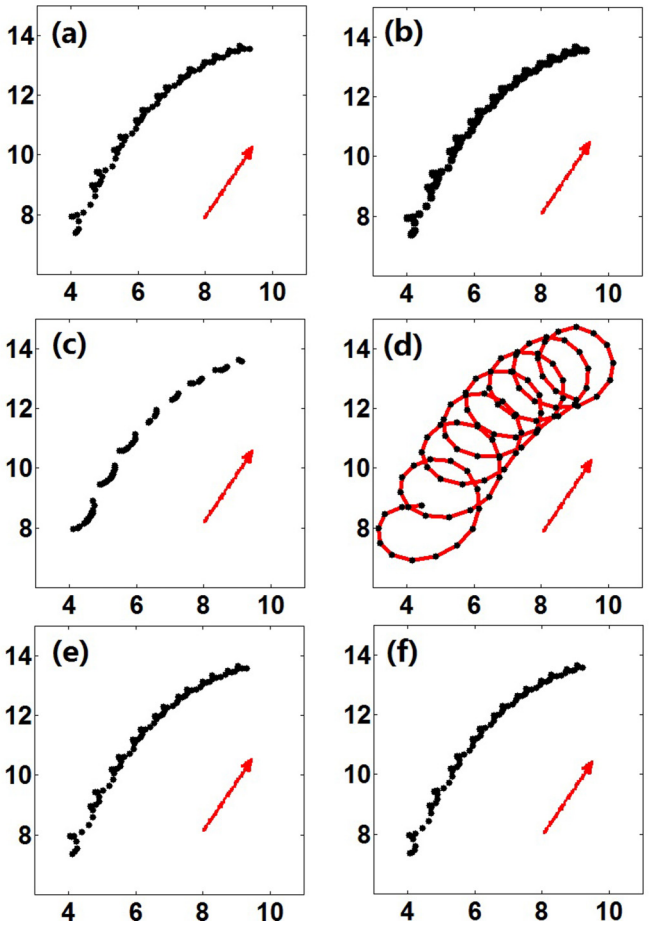

FIG. 3. Six methods of identifying the PS in a time duration 100; the parameters are the same as in Fig. 1. The time interval of the PS detection is 1 and the time delay $\tau = 0.1T$. (a) Using the simplified phase-integral method; (b) using the convolution method; (c) using the location-centric method; (d) using the Jacobian-determinant method; (e) using the zero-normal-velocity method II; (f) using the zero-normal-velocity method I which is not related to τ.

Next we consider rigidly rotating (stationary) spiral waves. For simplicity, model parameters are chosen the same as in Fig. 1 except that parameter β is tuned to 0.78, with which one can get $V^* = -1.256$ by using the software DXSPIRAL. Table I also shows PS-detecting error rates of different methods and time delays with stationary spiral waves. The location-centric

TABLE I. PS-detecting error rates. The zero-normal-velocity method I is not related to τ.

	Nonstationary		Stationary	
Time delay τ	$0.05T$	$0.1T$	$0.05T$	$0.1T$
Simplified phase-integral method	0	0	0	0
Convolution method	0	0	0	0
Location-centric method	86%	67%		
Jacobian-determinant method	0	0	0	0
Zero-normal-velocity method II	0	0	0	0
Zero-normal-velocity method I	0		0	

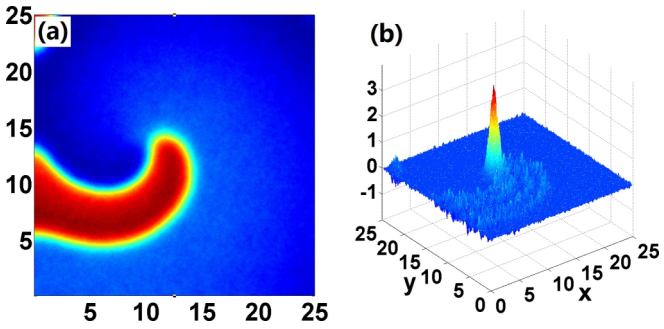

FIG. 4. The effect of noise. (a) A snapshot of the spatial distribution of the fast variable η. (b) Numerical values of the modified Jacobian determinant $D(V/x)$. The noise amplitude $\eta = 0.003$ and the other parameters are the same as those in Fig. 1.

method fails to detect any PS, due to the usage of the location-centric method being limited on the condition that voltage changes continuously over time as mentioned in [30]. Nevertheless, other methods show their robustness with different choices of time delays, since in all cases the error rates are 0.

Furthermore, we also explored the influence on PS tracking with a bigger time delay such as $\tau = 0.25T$. For nonstationary spiral waves, the performance of the PS identification is similar to $\tau = 0.05T$ or $\tau = 0.1T$. However, for the stationary case with the chosen model and parameters, the simplified phase-integral method, the convolution method, the location-centric method, the Jacobian-determinant method, and the zero-normal-velocity method II experience problems since phase loops cross over in reconstructed state space and phase cannot be defined uniquely, such as in Fig. 2(a) of Ref. [28].

B. Effect of noise

There are many realistic situations in which noise cannot be neglected [49,28]. In order to study the effect of noise on localizing PSs in model simulations, we add spatiotemporal white noise $\sigma(x, y, t)$ [49] to the right-hand side of Eq. (1a), in which $\langle\sigma(x, y, t)\rangle = 0$, $\langle\sigma(x, y, t)\sigma(x', y', t')\rangle = \eta\delta(x - x')\delta(y - y')\delta(t - t')$. To decrease the effect of noise, we can use a modified Jacobian determinant:

$$D(V/x)_{i,j} = \sum_{i'=i-2}^{i+2} \sum_{j'=j-2}^{j+2} D(V/x)_{i'j'}.$$

That is, now the value of $D(V/x)$ at site (i, j) is replaced by the mean value of $D(V/x)$ at adjacent sites. Spatial distributions of the fast variable V and the modified Jacobian determinant in the presence of noise are shown in Fig. 4. One can see that the Jacobian determinant $D(V/x)$ gets bumpy in the presence of noise; however, $D(V/x)$ is still localized at the PS and it takes its extremum approximately at the PS. The PS position for the spiral still can be identified by finding the site where $D(V/x)$ takes its extremum.

When the noise is very weak, e.g., the noise amplitude $\eta = 1.0 \times 10^{-10}$, the PS-detecting error rates of all the methods do not vary and are the same as in Table I. However, when we increase η to 0.003, most of the PS-detecting error rates increase, while the error rate of the Jacobian-determinant method is zero. When we further increase η to 0.009, the error rates of other methods are high while the error rate of the Jacobian-determinant method is still zero (see Table II for details). The zero-normal-velocity method I is very sensitive to noise: When the noise amplitude $\eta = 1.0 \times 10^{-9}$, the PS-detecting error rate is already 42%. The zero-normal-velocity method II is not sensitive to noise, the same as the simplified phase-integral method and the convolution method. The reasons are as follows: The zero-normal-velocity method II is equivalent to the phase-integral method, while the zero-normal-velocity method I is equivalent to the phase-integral method in the case of $\tau \ll 1$ (for details, please see the Appendix).

TABLE II. PS-detecting error rates with spatiotemporal white noise. The spiral is nonstationary and the time delay $\tau = 0.1T$. The zero-normal-velocity method I is not related to τ.

	$\eta = 0.003$	$\eta = 0.009$
Simplified phase-integral method	5%	100%
Convolution method	7%	100%
Location-centric method	71%	100%
Jacobian-determinant method	0	0
Zero-normal-velocity method II	8%	100%
Zero-normal-velocity method I	100%	100%

C. Multiple spiral waves

During fibrillation, multiple rotating waves are often observed on the heart. Now, we consider a larger system ($Lx = Ly = 50$, consisting of 1000×1000 grid points) where there coexist three spiral waves [two clockwise spirals and one counterclockwise spiral; see Fig. 5(a)]. In Fig. 5(b), we numerically calculated the values of the Jacobian determinant $D(V/x)$ according to Eq. (5). One can see that $D(V/x)$ takes its extremum approximately at the three PSs, while it is almost zero in other regions. For the counterclockwise spiral $D(V/x)_{\rm PS} > 0$, while for the two clockwise ones $D(V/x)_{\rm PS} < 0$. The trajectories of the three PSs produced by the Jacobian-determinant method are shown in Fig. 5(c) and the error rate of the PS detection is 0.

D. Effect of spatial resolution

Optical and electric mapping are two well-known methods that are commonly used for acquiring electrograms during fibrillation. The optical mapping method has been capable of recording the transmembrane potential from thousands of sites over the whole heart with high spatial and temporal resolution [5,50]. However, clinical usage of optical mapping in humans may not be available due to the toxicity of the required voltage-sensitive dyes. In the electric mapping approach, the surface of the heart (epicardium and/or endocardium) is brought in contact with an array of unipolar and/or bipolar electrodes with necessary acquisition hardware and analyzed using specific software. In clinical usage, although mapped with several electrodes in an array, the spatial resolution, i.e., number of electrodes per unit area, is usually inadequate to represent every single point on the surface of the heart [34,51].

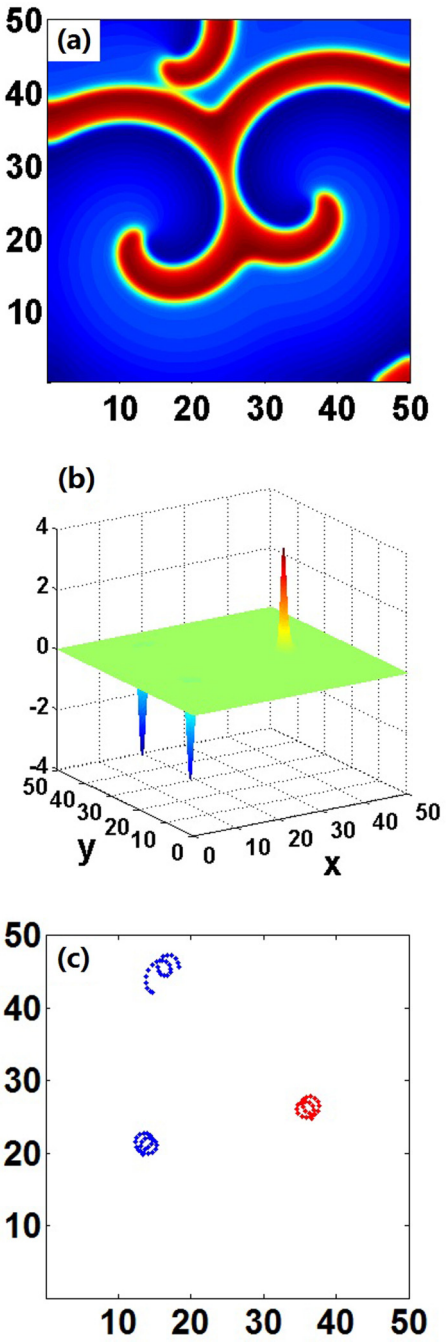

FIG. 5. The Jacobian-determinant method of identifying multiple PSs. A time delay $\tau = 0.1T$ and an instant time $t = 15$ are chosen. The model and its parameters are the same as in Fig. 1. (a) A snapshot of the spatial distribution of the fast variable V. (b) Numerical values of the Jacobian determinant $D(V/x)$. (c) PS trajectories of the three meandering spiral waves in a time duration 25. The blue and the red dots correspond to the PSs of the clockwise and the counterclockwise spirals, respectively.

If Fig. 1(a) (500 × 500 pixels) is taken as an example of a real system, then Fig. 6(a) (50 × 50 pixels) could be viewed as a map of voltage data recorded by the electrodes placed on the surface of the heart. The pixels of Fig. 6(a) are much fewer than those of Fig. 1(a), since only 1% of the data from the real system are recorded. However, the basic property of the

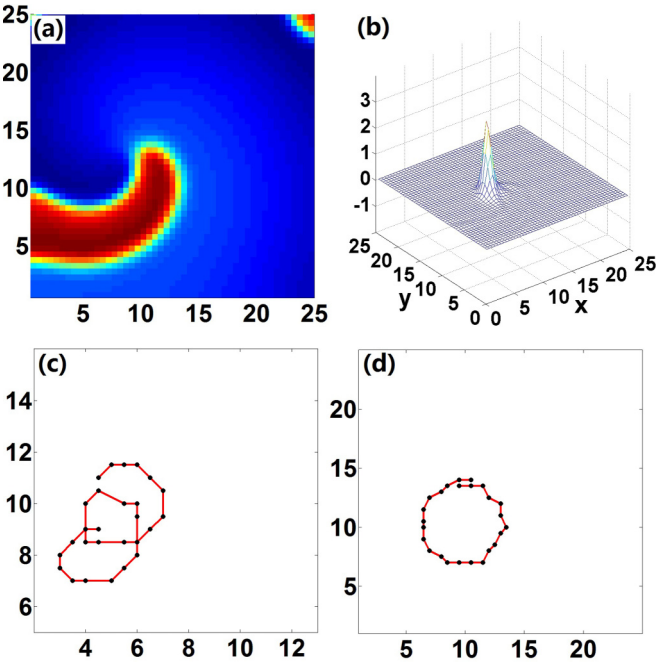

FIG. 6. The spatial resolution of the fast variable V is decreased to 50 × 50 pixels. The parameters are the same as in Fig. 1, except in (d) parameter β is tuned to 0.78. (a) A snapshot of the spatial distributions of the fast variable V and the same instant time $t = 90$ is chosen as in Fig. 1. (b) Numerical values of $D(V/x)$ at $t = 90$. (c) Tip trajectories of a meandering spiral wave. (d) Tip trajectories of a rigidly rotating spiral wave.

Jacobian determinant still remains as we can see in Fig. 6(b): $D(V/x)$ is still localized at the PS. PS trajectories are shown in Fig. 6(c), which is similar to Fig. 3(d). We also studied a rigidly rotating spiral wave, and the PS trajectories are shown in Fig. 6(d), which shows this method works well, too.

In order to study the effect of spatial resolution in detail, we investigate the PS-detecting error rates for different spatial resolutions in Table III: 64 × 64, 32 × 32, 16 × 16, and 8 × 8.

TABLE III. PS-detecting error rates of the Jacobian-determinant method for different spatial resolutions. The spiral is stationary.

τ	64 × 64	32 × 32	16 × 16	8 × 8
$0.01T$	23%	50%	98%	92%
$0.02T$	0	4%	87%	91%
$0.03T$	0	0	51%	89%
$0.04T$	0	0	4%	89%
$0.05T$	0	0	0	88%
$0.06T$	0	0	0	86%
$0.07T$	0	0	0	84%
$0.08T$	0	0	0	79%
$0.09T$	0	0	0	37%
$0.10T$	0	0	0	8%
$0.11T$	0	0	0	0
$0.12T$	0	0	0	0
$0.13T$	14%	10%	8%	5%
$0.14T$	24%	66%	77%	34%
$0.15T$	63%	85%	90%	59%

For simplicity, we only consider the stationary spirals. One can see that the zero error rate region for the time delay τ becomes narrow as we decrease the spatial resolution. Note that only 8×8 electrodes are available in clinical usage currently [14] and in this case the error rate of the Jacobian-determinant method is low only for $\tau \in [0.10\mathrm{T}, 0.13\mathrm{T}]$.

E. Cardiac model

In order to ensure that the Jacobian-determinant method of localizing PSs can be applied to cardiac data, we analyze spiral waves generated with the Luo-Rudy model [52]:

$$\frac{\partial V}{\partial t} = -\frac{I_{\mathrm{ion}}}{C_m} + \nabla \cdot (D \nabla V), \tag{9}$$

where V is the membrane potential; $C_m = 1\,\mu\mathrm{F/cm}^2$ is the membrane capacitance; $D = 0.001\,\mathrm{cm}^2/\mathrm{ms}$ is the diffusion current coefficient; the total ionic currents I_{ion} are determined by ionic gates, whose gating variables are obtained as solutions to a coupled system of nonlinear ordinary differential equations; and the parameters are simplified as in Ref. [53]. The Luo-Rudy model is integrated on the 3 cm $\times$ 3 cm medium with no-flux boundary conditions via the Euler method. The space and the time step are $\Delta x = 0.0075\,\mathrm{cm}$, $\Delta y = 0.0075\,\mathrm{cm}$, and $\Delta t = 0.00125\,\mathrm{ms}$, respectively.

A meandering clockwise spiral is considered and the spatial distribution of the membrane potential V at an instant time $t = 90\,\mathrm{ms}$ is shown in Fig. 7(a). In Fig. 7(b), the middle red and blue isolines are the values of $V(t)$ and $V(t+\tau)$ of the grid that reaches the minimum of $D(V/x)$ [Fig. 7(c)], respectively. The intersection of those two middle lines is the PS. Near the PS, the isolines of $V(t)$ and $V(t+\tau)$ cross each other, which is the same as the spiral of FHN in Fig. 1(c). The PS of the clockwise spiral is distinguished by its sharp local minimum of $D(V/x)(n_t = \mathrm{sgn}[D(V/x)_{\mathrm{PS}}] = -1)$. In Fig. 7(d), the PS positions for the clockwise spiral are identified by minimizing $D(V/x)$ [or by maximizing $|D(V/x)|$] and the PS-detecting error rate is 0.

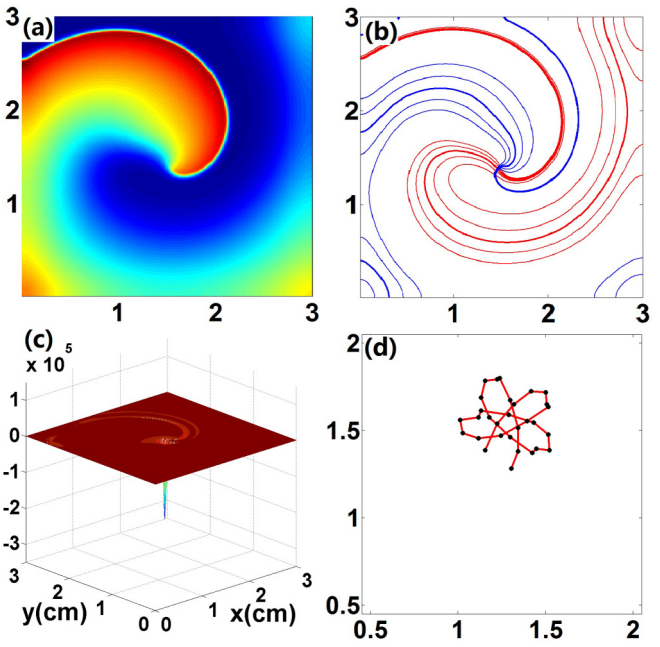

FIG. 7. The Luo-Rudy model is used; a time delay $\tau = 5\,\mathrm{ms}$ and an instant time $t = 90\,\mathrm{ms}$ are chosen. All parameters are chosen the same as those in Fig. 3A(a) in Ref. [53]. (a) A snapshot of the spatial distributions of the membrane potential V. (b) The middle red isoline $V(t) = -68.68\,\mathrm{mv}$ is the value of V of the grid that reaches the minimum of $D(V/x)$, and the other four red isolines are $V(t) \pm \Delta V$ and $V(t) \pm 2\Delta V$. Similarly, the middle blue isoline and the other four blue isolines correspond to $V(t+\tau) = -37.63\,\mathrm{mv}$, $V(t+\tau) \pm \Delta V$, and $V(t+\tau) \pm 2\Delta V$, respectively. $\Delta V = 5\,\mathrm{mv}$ is chosen in both the red and blue cases. (c) Numerical values of the Jacobian determinant $D(V/x)$. (d) The trajectory of the PS obtained by the Jacobian-determinant method in a time duration 150 ms. The time interval of the PS detection is 5 ms.

IV. DISCUSSION

All the above discussed methods except the Jacobian-determinant method require choosing the state space origin V^*. One can see that the simplified phase-integral method, the convolution method, the zero-normal-velocity method II, and the zero-normal-velocity method I have a 0 error rate of the PS detection when we use the best choice of the state space origin V^*. In Ref. [33], Gray and colleagues pointed out that the choice of V^* influences the identification of the PS. For example, inappropriate origin choice can lead to an error in the identification of the number and the lifetime of spiral waves. In Ref. [20], Nattel and colleagues showed clearly that the state space origin V^* for contour-line establishment is crucial for appropriate tracking of the PSs of rapidly rotating waves. Too high a state space origin may result in missing PSs and failing to follow them on a frame-to-frame basis. Too low a voltage threshold risks double detection of a wavelet. The best choice of the state space origin can be obtained for simple models such as FHN; however, in realistic cardiac myocyte models and in experiments, V^* is hard to obtain [33]. Here, one can see that an advantage of the Jacobian-determinant method is that V^* is not needed. Another advantage of the Jacobian-determinant method is that the local phase $\phi(x, y, t)$ does not need to be calculated and this would be convenient for the purposes of PS tracking, since the definition of phase can vary from study to study [11,27,33,35,36].

V. CONCLUSION

We found that the Jacobian determinant $D(V/x)$ in the reconstructed state space takes its extremum approximately at the PSs, while it is almost zero in other regions. In other words, the PSs are distinguished by their sharp local extrema of $D(V/x)$. This property provides an identification of the PS positions by maximizing $|D(V/x)|$. It is a counterclockwise spiral when $D(V/x)_{\mathrm{PS}} > 0$ (i.e., $n_t = +1$) and a clockwise one when $D(V/x)_{\mathrm{PS}} < 0$ (i.e., $n_t = -1$). Using this method, we can identify the PSs within a very short time interval; this enables a description of spiral waves on a timescale much shorter than the period of rotation.

ACKNOWLEDGMENTS

We are grateful to S. M. Narayan and W.-J. Rappel for valuable discussions and comments on the manuscript, to M.-A. Bray for kindly providing the code of convolution method used in this paper for comparison and valuable discussions, to X. Gao and J.-T. Pan for helpful suggestions, and to the team that developed DXSPIRAL and made it publicly available. This work was supported by the National Natural Science Foundation of China under Grants No. 11675141 and No. 11775186, and the China Postdoctoral Science Foundation under Grant No. 2018M632444.

T.-C.L. and D.-B.P. contributed equally to this work.

APPENDIX

According to Eq. (2), the phase of the point (x, y), where

$$V(x, y, t) = V^*, \quad V(x, y, t + \tau) = V^*, \tag{A1}$$

is arbitrary. That is, the intersection of these two contours (A1) can be identified as the PS (see Fig. 1). Qu *et al.* used the method (A1) to calculate PS in Ref. [53]. Note that the method (A1) is equivalent to the phase-integral method [28] when the space steps $\Delta x,\ \Delta y \to 0$ [see Eq. (3) and Fig. 2].

When the time delay τ is extremely small, i.e., $\tau \ll 1$,

$$\partial_t V(x, y, t) = [V(x, y, t + \tau) - V(x, y, t)]/\tau + O(\tau).$$

Therefore, the method (A1) (in the case of $\tau \ll 1$) is equivalent to

$$V(x, y, t) = V^*, \quad \partial_t V(x, y, t) = 0,$$

which is just the zero-normal-velocity method I (7). In conclusion, the zero-normal-velocity method I (7) is equivalent to the phase-integral method (3) in the case of $\tau \ll 1$ and $\Delta x,\ \Delta y \to 0$.

On the other hand, $\partial_t V(x, y, t)$ in Eq. (7) is calculated according to $[V(x, y, t + \Delta t) - V(x, y, t)]/\Delta t$ where the time step $\Delta t \ll 1$. If we replace Δt by the time delay τ in Eq. (7), that is, $\partial_t V(x, y, t)$ is calculated roughly from $[V(x, y, t + \tau) - V(x, y, t)]/\tau$, the zero-normal-velocity method I (7) will change to the zero-normal-velocity method II (8) which is the same as the method (A1). Since the method (A1) is equivalent to the phase-integral method (3) when $\Delta x,\ \Delta y \to 0$, the zero-normal-velocity method II (8) will be equivalent to the phase-integral method (3) when $\Delta x,\ \Delta y \to 0$.

[1] A. T. Winfree, Science **175**, 634 (1972).
[2] V. K. Vanag and I. R. Epstein, Science **294**, 835 (2001).
[3] S. Jakubith, H. H. Rotermund, W. Engel, A. von Oertzen, and G. Ertl, Phys. Rev. Lett. **65**, 3013 (1990).
[4] S. Sawai, P. A. Thomason, and E. C. Cox, Nature (London, U. K.) **433**, 323 (2005).
[5] J. M. Davidenko, A. V. Pertsov, R. Salomonsz, W. Baxter, and J. Jalife, Nature (London, U. K.) **355**, 349 (1992).
[6] S. Luther, F. H. Fenton, B. G. Kornreich, A. Squires, P. Bittihn, D. Hornung, M. Zabel, J. Flanders, A. Gladuli, L. Campoy, E. M. Cherry, G. Luther, G. Hasenfuss, V. I. Krinsky, A. Pumir, R. F. Gilmour, Jr., and E. Bodenschatz, Nature (London, U. K.) **475**, 235 (2011).
[7] J. Christoph, M. Chebbok, C. Richter, J. Schröder-Schetelig, P. Bittihn, S. Stein, I. Uzelac, F. H. Fenton, G. Hasenfuß, R. F. Gilmour, Jr., and S. Luther, Nature (London, U. K.) **555**, 667 (2018).
[8] Z. Qu, G. Hu, A. Garfinkel, and J. N. Weiss, Phys. Rep. **543**, 61 (2014).
[9] S. Alonso, M. Bär, and B. Echebarria, Rep. Prog. Phys. **79**, 096601 (2016).
[10] S. Nattel, F. Xiong, and M. Aguilar, Nat. Rev. Cardiol. **14**, 509 (2017).
[11] R. A. Gray, A. M. Pertsov, and J. Jalife, Nature (London, U. K.) **392**, 75 (1998).
[12] R. A. Gray, J. Jalife, A. V. Panfilov, W. T. Baxter, C. Cabo, J. M. Davidenko, and A. M. Pertsov, Science **270**, 1222 (1995).
[13] R. A. Gray, J. Jalife, A. Panfilov, W. T. Baxter, C. Cabo, J. M. Davidenko, and A. M. Pertsov, Circulation **91**, 2454 (1995).
[14] S. M. Narayan, D. E. Krummen, K. Shivkumar, P. Clopton, W.-J. Rappel, and J. M. Miller, J. Am. Coll. Cardiol. **60**, 628 (2012).
[15] D. Barkley, M. Kness, and L. S. Tuckerman, Phys. Rev. A **42**, 2489 (1990).
[16] A. T. Winfree, Chaos **1**, 303 (1991).
[17] M. Hildebrand, M. Bär, and M. Eiswirth, Phys. Rev. Lett. **75**, 1503 (1995).
[18] I. V. Biktasheva, D. Barkley, V. N. Biktashev, and A. J. Foulkes, Phys. Rev. E **81**, 066202 (2010).
[19] J. Beaumont, N. Davidenko, J. Davidenko, and J. Jalife, Biophys. J. **75**, 1 (1998).
[20] R. Zou, J. Kneller, L. J. Leon, and S. Nattel, Chaos **12**, 764 (2002).
[21] F. Fenton and A. Karma, Chaos **8**, 20 (1998).
[22] R. Mandapati, Y. Asano, W. T. Baxter, R. Gray, J. Davidenko, and J. Jalife, Circulation **98**, 1688 (1998).
[23] Y. B. Liu, A. Peter, S. T. Lamp, J. N. Weiss, P.-S. Chen, and S.-F. Lin, J. Cardiovasc. Electrophysiol. **14**, 1103 (2003).
[24] F. H. Fenton, E. M. Cherry, H. M. Hastings, and S. J. Evans, Chaos **12**, 852 (2002).
[25] C. D. Marcotte and R. O. Grigoriev, Chaos **27**, 093936 (2017).
[26] F. Takens, Lect. Notes Math. **898**, 366 (1981).
[27] M.-A. Bray and J. P. Wikswo, Phys. Rev. E **65**, 051902 (2002).
[28] A. N. Iyer and R. A. Gray, Ann. Biomed. Eng. **29**, 47 (2001).
[29] M.-A. Bray, S.-F. Lin, R. R. Aliev, B. J. Roth, and J. P. Wikswo, Jr., J. Cardiovasc. Electrophysiol. **12**, 716 (2001).
[30] Y.-S. Lee, J.-S. Song, M. Hwang, B. Lim, B. Joung, and H.-N. Pak, PLoS One **11**, e0167567 (2016).
[31] R. FitzHugh, Biophys. J. **1**, 445 (1961).
[32] J. Nagumo, S. Arimoto, and S. Yoshizawa, Proc. IRE **50**, 2061 (1962).
[33] R. A. Gray, J. P. Wikswo, and N. F. Otani, Chaos **19**, 033118 (2009).

[34] K. Umapathy, K. Nair, S. Masse, S. Krishnan, J. Rogers, M. P. Nash, and K. Nanthakumar, Circ.: Arrhythmia Electrophysiol. **3**, 105 (2010).
[35] P. Kuklik, S. Zeemering, B. Maesen, J. Maessen, H. J. Crijns, S. Verheule, A. N. Ganesan, and U. Schotten, IEEE Trans. Biomed. Eng. **62**, 296 (2015).
[36] R. Vijayakumar, S. K. Vasireddi, P. S. Cuculich, M. N. Faddis, and Y. Rudy, Circ.: Arrhythmia Electrophysiol. **9**, e004409 (2016).
[37] N. D. Mermin, Rev. Mod. Phys. **51**, 591 (1979).
[38] A. Goryachev and R. Kapral, Phys. Rev. Lett. **76**, 1619 (1996).
[39] J. Davidsen, L. Glass, and R. Kapral, Phys. Rev. E **70**, 056203 (2004).
[40] J. T. Pan, M. C. Cai, B. W. Li, and H. Zhang, Phys. Rev. E **87**, 062907 (2013).
[41] H. Zhang, B. Hu, B. W. Li, and Y. S. Duan, Chin. Phys. Lett. **24**, 1618 (2007).
[42] Y. S. Duan and H. Zhang, Phys. Rev. E **60**, 2568 (1999).
[43] Y. S. Duan and M. L. Ge, Sci. Sin. **11**, 1072 (1979).
[44] D. Barkley, Phys. Rev. Lett. **68**, 2090 (1992).
[45] D. Barkley, V. N. Biktashev, I. V. Biktasheva, G. Bordyugov, and A. Foulkes, DXSPIRAL: A code for studying spiral waves on a disk, http://cgi.csc.liv.ac.uk/∼ivb/SOFTware/DXSpiral.html (2010).
[46] I. V. Biktasheva, D. Barkley, V. N. Biktashev, G. V. Bordyugov, and A. J. Foulkes, Phys. Rev. E **79**, 056702 (2009).
[47] P. Bittihn, S. Berg, U. Parlitz, and S. Luther, Chaos **27**, 093931 (2017).
[48] M.-A. Bray (private communication).
[49] J. Garcia-Ojalvo and J. M. Sancho, *Noise in Spatially Extended Systems* (Springer, New York, 1999).
[50] W. T. Baxter, J. M. Davidenko, L. M. Loew, J. P. Wuskell, and J. Jalife, Ann. Biomed. Eng. **25**, 713 (1997).
[51] W.-J. Rappel and S. M. Narayan, Chaos **23**, 023113 (2013).
[52] C. H. Luo and Y. Rudy, Circ. Res. **68**, 1501 (1991).
[53] Z. Qu, F. Xie, A. Garfinkel, and J. N. Weiss, Ann. Biomed. Eng. **28**, 755 (2000).